Original Article
Differential molecular response of larynx cancer cell lines to combined VPA/CDDP treatment

Ewelina Gumbarewicz[1], Przemko Tylżanowski[1,2], Jarogniew Łuszczki[3], Joanna Kałafut[1], Arkadiusz Czerwonka[1], Justyna Szumiło[4], Anna Wawruszak[1], Krzysztof Kupisz[5,6], Krzysztof Polberg[7], Jolanta Smok-Kalwat[8], Andrzej Stepulak[1]

[1]Department of Biochemistry and Molecular Biology, Medical University of Lublin, Chodzki 1 St., 20-093 Lublin, Poland; [2]Laboratory for Developmental and Stem Cell Biology, Department of Development and Regeneration, Skeletal Biology and Engineering Research Centre, University of Leuven, Leuven, Belgium; [3]Department of Pathophysiology, Medical University, Lublin, Poland; [4]Department of Clinical Pathomorphology, Medical University of Lublin, Lublin, Poland; [5]Department of Otolaryngology and Laryngeal Oncology, Medical University of Lublin, Lublin, Poland; [6]Department of Otolaryngology, Center of Oncology of The Lublin Region, Lublin, Poland; [7]Department of Otolaryngology, MSWiA Hospital, Lublin, Poland; [8]Department of Clinical Oncology, Holycross Cancer Centre, Kielce, Poland

Abstract: Successful treatment of advanced larynx squamous cell carcinoma (LSCC) remains a challenge, mainly due to limited response to chemotherapy and the phenomenon of the drug resistance. Therefore, new chemotherapeutic solutions are needed. The aim of this study was to explore benefit of combined cisplatin (CDDP) and valproic acid (VPA) therapy in patients' derived LSCC cell lines. Cell viability assay was used to establish cellular response to the drug by isobolography followed by RNA sequencing (RNAseq) analysis. *Danio rerio* were used for *in vivo* studies. Depending on the cell line, we found that the combinations of drugs resulted in synergistic or antagonistic pharmacological interaction, which was accompanied by significant changes in genes expression profiles. The presented therapeutic scheme efficiently blocked tumor growth in an *in vivo* model, corresponding to the in vitro performed studies. Interestingly the RK5 cell line, upon the combined treatment acquired a molecular profile typically associated with epithelial to mesenchymal transition (EMT). Hence, our studies demonstrates that patient-specific personalized therapy of larynx cancer should be considered and the combination of cisplatin and valproic acid should be explored as a potential therapeutic strategy in the treatment of larynx cancer.

Keywords: Laryngeal cancer, cisplatin, valproic acid, gene expression

Introduction

Laryngeal squamous cell carcinoma (LSCC) is the most common tumor of the upper aerodigestive tract, with more than 13,000 new cases in US every year. LSCC is still associated with high morbidity and mortality, especially in its advanced stage [1]. Since the functional organ preservation (larynx) is clinically preferred, the combination of chemotherapy and radiation therapy (RT) is widely recommended. Different clinical regimes are used including the induction chemotherapy prior to surgery or RT; concurrent chemoradiotherapy, or sequential therapy - the combination of induction chemotherapy followed by concurrent chemoradio-

therapy [2, 3]. However, chemotherapy of advanced larynx cancer-bearing patients did not change significantly over the years. Currently, treatment of LCSC is most frequently based on the use of cisplatin (cis-diamminedichloridoplatinum, CDDP) or its derivatives, which are still the most commonly used chemotherapeutic agents in LSCC in spite of conferring only a minor overall survival benefit [4]. Unfortunately, platin-derivatives develop many undesirable side effects, including neuro- and ototoxicity (peripheral neuropathy, hearing loose, tinnitus), pulmonary complications, nephrotoxicity, hypogonadism and premature hormonal aging, and cognitive impairment [5] which drastically reduces patient's comfort of

life. Introduction of new therapeutic approaches, including immunotherapy and epidermal growth factor receptor (EGFR)-directed antibodies (Cetuximab) or EGFR tyrosine kinase inhibitors failed to improve outcome of larynx cancer patients, despite high EGFR expression in these tumors [6-8]. Equally, no targeted agents and radiosensitizers studied were shown effective [9]. Additionally, frequent development of chemoresistance to cisplatin results in treatment failure. Thus, it becomes apparent that there is unmet need for new pharmacological solutions to this type of cancer.

Epigenetic alterations, including acetylation/deacetylation of histones, play a pivotal role in initiation and progression of many cancers [10], including LSCC [11]. It has been reported, that histone deacetylase inhibitors (HDIs) have emerged as promising chemotherapeutic agents by inducing a wide range of cellular responses including induction of apoptosis and cell cycle arrest [12]. HDIs mechanism of action was attributed to induction of apoptosis and cell cycle arrest of larynx cancer cells, presumably by upregulation of CDKN1A and downregulation of CCND1 encoding p21WAF1/CIP1 and cyclin D1 proteins, respectively, as presented previously in our [13, 14] and other studies [15].

One of these agents - Valproic acid (VA), a short-chain fatty acid, which until now has been widely used for the treatment of selected types of epilepsy, bipolar disorders and migraine, received a new attention with the discovery of its new molecular mode of action - inhibition of histone deacetylase (HDAC) enzymes class I and class IIa. Depending on the cellular and tissue context, VPA has been shown to induce apoptosis, inhibit cancer cells proliferation and tumor angiogenesis, as well as epithelial to mesenchymal transition (EMT) [16, 17]. It has been also shown that VPA enhanced cisplatin sensitivity of non-small cell lung cancer cells [18] or re-sensitized cisplatin-resistant ovarian cancer cells [19] to CDDP therapy. The last observation suggests that VPA might overcome the common clinical problem of drug-resistance. Given the fact, that VPA induces minimal cytotoxic effects with regard to normal cells [20, 21], and is well tolerated by patients [22], its use in combination with standard chemotherapeutic agents may be useful application for cancer treatment. Respective clinical trial is ongoing [23].

The aim of our study was to explore the possibility of synergy between VAP and CDDP in treating the laryngeal cancer. We used a model based on patient-derived cell lines and investigated the response to the combined treatment using isobolography to establish the type of pharmacologic interaction between CDDP and VPA. Additionally, we investigated the molecular response of the cell line to the treatment by using RNA Seq. Depending on the cell line, the combinations of drugs resulted in synergistic or antagonistic pharmacologic interaction, accompanied by significant changes in genes expression profiles demonstrated by RNA sequencing analysis. Our results demonstrate that VPA could improve CDDP-mediated treatment of larynx cancer cells *in vitro* in some cases underscoring the critical need for personalized therapy for larynx cancer patients.

Materials and methods

Reagents

VPA and CDDP were purchased from Sigma (St. Louis, MO, USA), and dissolved in phosphate buffered saline (PBS) with Ca^{2+} and Mg^{2+} at 100 mM and 1 mg/ml concentrations as stock solutions, respectively. The drugs were diluted to the respective concentration with culture medium just before use.

Cell lines

Human larynx cancer cell lines (RK33 and RK45) were obtained from laryngeal cancer cells derived from patients with diagnosed laryngeal squamous cell carcinoma. Both patients displayed identical advancement of the disease (T3N0M0). Cancer tissue was removed from the larynx after total laryngectomy, and cell lines were established without immortalizing techniques. The characterization of RK33 and RK45 cell lines has been published [24]. Despite growing for many passages on plastic surfaces, both cell lines exhibit similar histologic features, characteristic for squamous cell carcinomas (**Figure 3A**, **3B**). Larynx cancer cell lines were grown using RPMI 1640 culture media (Sigma) with 10% Fetal Bovine Serum (FBS) (Sigma), penicillin (100 µg/ml) (Sigma) and streptomycin (100 µg/ml) (Sigma). Mycoplasma-free cultures were maintained at 37°C in 5% CO_2.
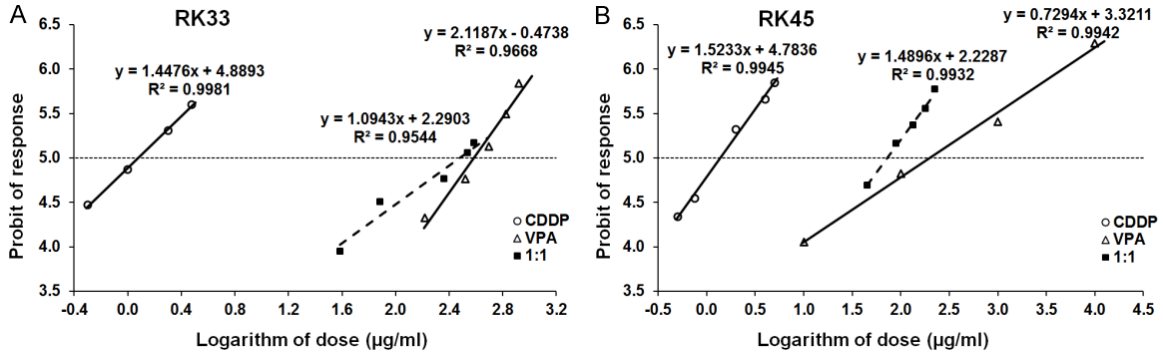
Figure 1. A, B. Log-probit dose-response effects for cisplatin (CDDP) and valproic acid (VPA) administered separately, and in combination at the fixed drug dose ratio of 1:1, illustrating the anti-proliferative effects of the tested drugs in the cancer cell lines RK33 and RK45, as measured *in vitro* by the MTT assay.
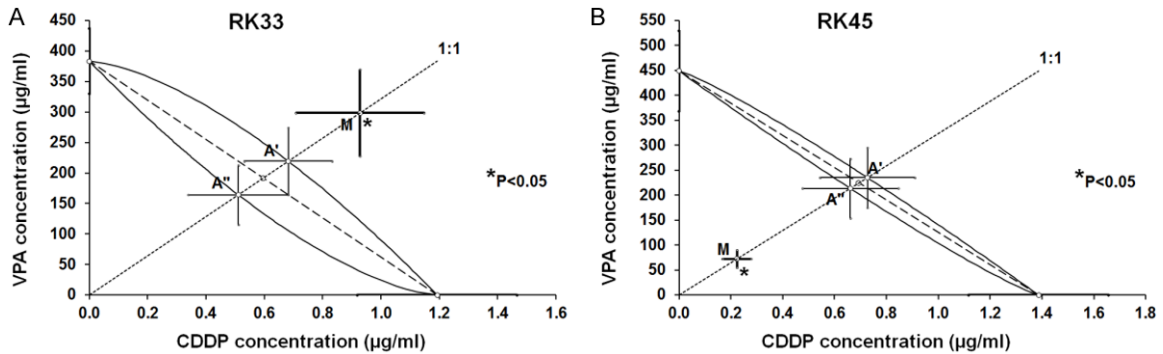
Figure 2. A, B. Isobolograms documenting interactions between cisplatin (CDDP) and valproic acid (VPA) with respect to their anti-proliferative effects in two cancer cell lines RK33 and RK45, as measured *in vitro* by the MTT assay. Median inhibitory concentrations (IC_{50} ± S.E.M.) for CDDP and VPA are plotted graphically on the X- and Y-axes, respectively. Lower and upper isoboles of additivity represent the curves connecting the IC_{50} values for CDDP and VPA. The dotted line starting from the point (0, 0) indicates the fixed drug dose ratio combination of 1:1. Points A' and A" depict the theoretically calculated $IC_{50\ add}$ values (± S.E.M. as horizontal and vertical error bars) for both, upper and lower isoboles of additivity, respectively. Point M illustrates the experimentally-derived $IC_{50\ mix}$ (± S.E.M. as horizontal and vertical error bars) value for total dose of the mixture that produced a 50% anti-proliferative effect in two cancer cell lines RK33 and RK45, as measured *in vitro* by the MTT assay. A. The experimentally-derived $IC_{50\ mix}$ value (the point M) is placed significantly above the point A', indicating sub-additive (antagonistic) interaction between CDDP and VPA for the cancer cell line RK33. *P<0.05 vs. the respective $IC_{50\ add}$ values. B. The experimentally-derived $IC_{50\ mix}$ value (the point M) is placed significantly below the point A", indicating supra-additive (synergistic) interaction between CDDP and VPA for the cancer cell line RK45. *P<0.05 vs. the respective $IC_{50\ add}$ values.

Hematoxylin-eosin staining

The RK33 and RK45 cells at a density of 5 × 10^5 cells/mL were seeded on 8 wells Nunc™ Lab-Tek™ II Chamber Slide™ System (Corning) which consists of a removable polystyrene media chamber attached to a standard glass slide. At confluence of 80%, the cells were fixed in 99,5% ice-cold acetone for 1 min and washed with water. After added with hematoxylin for 3 min and washed with water, the slides were subsequently dyed with eosin, dehydrated with gradient ethanol, acetone, soaked with xylene and mounted with neutral balsam.

Cell viability assay

Cancer cell lines were plated on 96-well microplates at a density of 1 × 10^4 cells/ml (RK33) and 3 × 10^4 cells/ml (RK45). The cell viability was determined using the MTT assay as we described previously [13].

Isobolographic analysis

Isobolographic analysis was performed in a strict accordance to the method as described previously [14]. To begin isobolographic analysis of interaction between CDDP and VPA, we
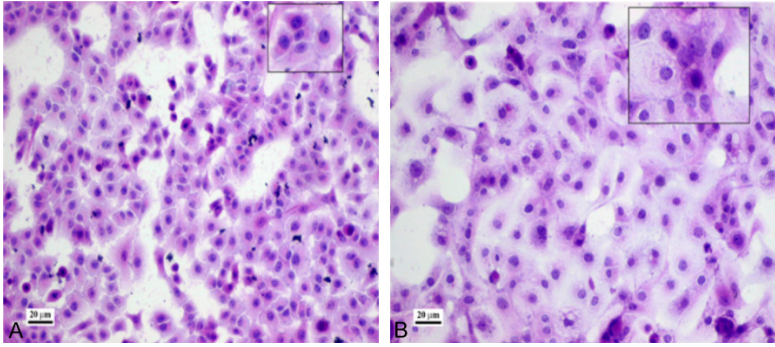
Figure 3. Morphology of laryngeal squamous cell carcinoma-derived (A) RK33 and (B) RK45 cell lines (hematoxylin and eosin stain, objective magnification 20x). (A) Cells are medium-sized, polygonal with abundant, eosinophilic cytoplasm and round to oval nuclei with a few small nucleoli. Some more spindle-shaped cells are seen as well. Sparse mitotic figures are noted. Cells are cohesive, forming solid sheath, adenoid structures and small Island; (B) Cells are medium-sized or large, polygonal with abundant pale or weakly eosinophilic cytoplasm and round to oval nuclei with a few small nucleoli. Some more spindle-shaped cells are seen and occasionally, giant multinucleated. Sparse mitotic figures are noted. Cells are cohesive, forming solid sheath and small islands.

Table 1. Anti-proliferative effects of CDDP and VPA administered singly in two cancer cell lines RK33 and RK45 as measured *in vitro* by the MTT assay

Cell line	Drug	IC_{50} (µg/ml)	*n*
RK33	CDDP	1.193 ± 0.273	96
RK33	VPA	383.4 ± 53.73	120
RK45	CDDP	1.387 ± 0.270	120
RK45	VPA	449.1 ± 80.79	72

Median inhibitory concentrations (IC_{50} values in µg/ml ± S.E.M.) of CDDP and VPA were determined experimentally in two cancer cell lines. *n* - total number of measurements used at those concentrations whose expected anti-proliferative effects ranged between 4 and 6 probits (16% and 84%).

$IC_{50\ add}$ values, according to the methods described elsewhere [26, 27]. Theoretically, four types of interaction can be distinguished, as follows: supra-additivity (synergy), additivity, sub-additivity (relative antagonism) and infra-additivity (absolute antagonism) [28].

Statistical analysis

Linear log-probit analysis allowed us to calculate the experimentally-derived IC_{50} and $IC_{50\ mix}$ values for CDDP, VPA and their combination at the fixed drug dose ratio of 1:1 in two cancer cell (RK33 and RK45) lines, as described earlier in more detail [25, 29]. Statistical difference between the experimentally-derived $IC_{50\ mix}$ values and the theoretically calculated additive $IC_{50\ add}$ values was verified with unpaired Student's t-test, as presented elsewhere [30]. To analyze the data, GraphPad Prism 5.0 software with one-way ANOVA and the Tukey-Kramer post-hoc test were used. Statistical significance was established at P<0.05.

RNA sequencing analysis

Cells were grown on 6-well plates for 24 hours and subsequently treated with CDDP and VPA at IC_{50} does for 24 hours. RNA was extracted according to RNeasy Mini Kit protocol (Qiagen). Following the RNA extraction, the samples were processed using Illumina Trueseq mRNA kit and sequences using HiSeq4000 instrument (Illumina). Two biological replicates for RK45 and three biological replicates for RK33 were processed. Following the sequencing, the samples were aligned using HiSat2 [31] and the count files were generated using HTSEQ [32]. The identification of the differentially expressed gens was done using DSEQ2 [33] in R environment (https://www.r-project.org/).

Zebrafish xenograft injection

Adult zebrafish (*Danio rerio*) were raised at 28.5°C under a 14 h of light and 10 h of dark cycle. Embryos were maintained in E3 buffer.

determined inhibition of cell viability of RK33 and RK45 cancer cell lines along with increasing doses of CDDP and VPA used singly. From log-probit dose-response effects for CDDP and VPA in both, RK33 and RK45 cell lines we calculated median inhibitory concentrations (IC_{50} values) for CDDP and VPA, as recommended earlier [25]. Because the dose-response effects for CDDP and VPA in both, RK33 and RK45 cell lines were non-parallel (**Table 1**), a type I isobolographic analysis for non-parallel dose-response effect curves was used [26]. The type of interactions between CDDP and VPA was established by comparing the experimentally determined $IC_{50\ mix}$ values (at the fixed-ratio of 1:1) with the theoretically calculated additive

Table 2. Type I isobolographic analysis of interactions (for non-parallel dose-response effects) between CDDP and VPA in two cancer cell lines RK33 and RK45 as measured in vitro by the MTT assay

Cell line	Combination	$IC_{50\,mix}$ (μg/ml) n_{mix}	$^{L}IC_{50\,add}$ (μg/ml)	n_{add}	$^{U}IC_{50\,add}$ (μg/ml)	n_{add}
RK33	CDDP+VPA	383.4 ± 53.73 * 120	164.5 ± 48.72	212	220.0 ± 55.36	212
RK45	CDDP+VPA	72.52 ± 17.70 * 80	214.5 ± 59.58	236	236.0 ± 60.03	236

Median inhibitory concentrations (IC_{50} values in μg/ml ± S.E.M.) for the mixture of CDDP+VPA were determined both, experimentally ($IC_{50\,mix}$) and theoretically calculated ($IC_{50\,add}$) from the equations of additivity for a 50% inhibition of cell proliferation in two cancer cell lines RK33 and RK45. n_{mix} - total number of items used at those concentrations whose expected anti-proliferative effects ranged between 16% and 84% (i.e., 4 and 6 probits) for the experimental mixture; n_{add} - total number of measurements calculated for the additive mixture of the drugs examined ($n_{add} = n_{\_CDDP} + n_{\_VPA}$ - 4); $^{L}IC_{50\,add}$ and $^{U}IC_{50\,add}$ - are IC_{50} values (in μg/ml ± S.E.M.) calculated from the equations for the lower and upper isoboles of additivity, respectively. The unpaired Student's t-test was used to statistically analyze the data. *P<0.05 vs. the respective $IC_{50\,add}$ values.

Cancer cell lines were cultured at 34°C about one month before injection. Cultured cancer cells were labeled with Vybrant DiD (Invitrogen) according to the manufacturer protocol. Stained cells were resuspended in DMEM at the final concentration of 1×10^{7} cells/ml. Zebrafish larvae was manually dechorionated and injected 48 h postfertilization (hpf). Cancer cells were loaded into a borosilicate glass needle pulled by a P-1000 Next Generation Micropipette Puller (Sutter Instrument Company). 200 labelled cells were injected into interior yolk space of each larvae using an electronically regulated air-pressure microinjector (Narishige IM-300 Microinjector). After injection, zebrafish with the xenografts were cultured at 34°C until the end of experiments. At 24 h postiniection (hpi), the zebrafish larvae with transplanted cells were collected and randomly assigned to drug treatment and control groups.

In vivo imaging

The zebrafish larvae were anaesthetized by 0.04 mg/ml ethyl 3-aminobenzoate methanesulfonate tricaine before imaging. Images of xenografts were acquired 24, 48, 72 and 96 hpi using an EVOS M5000 Imaging System with the filter Cy5 (excitation: 628 nm; emission: 692 nm). Xenografts areas were quantified with the Ilastik and Fiji software (ImageJ) according to Naakka et al [34].

RNA extraction and quantitative analysis

Total RNA from 25 fish with xenograft in each studied group was isolated using ExtractMe Total RNA kit (Blirt) according to the manufacturer protocol. The isolated RNA was used for cDNA synthesis through High-Capacity cDNA Reverse Transcription Kit with addition of a RNase Inhibitor (Applied Biosystems). *Zebrafish*

glyceraldehyde 3-phosphate dehydrogenase (*gapdh: forward 5'-GTGGAGTCTACTGGTGTC-TTC-3', revers 5'-GTGCAGGAGGCATTGCTTACA-3'*) was used as a housekeeping gene. The human *GAPDH* gene (forward 5'-CTCTGCTCCT-CCTGTTCGAC-3', revers 5'-GCCCAATACGACCA-AATCC-3') was used to quantify the number of human cells in the injected zebrafish larvae. Quantitative real-time PCR (qPCR) expression analysis were then performed with the LightCycler® 480 II instrument (Roche) in triplicates on 96 well plates using PowerUp SYBR Green Master Mix (Applied Biosys-tems). Relative mRNA expression was calculated using the delta CT subtraction and normalized to the expression of *gapdh*.

Results

Anti-proliferative effects of CDDP and VPA administered separately or combined together to the RK33 and RK45 cell lines

We found that CDDP, VPA and their combination at the fixed-ratio of 1:1 decreased, in a dose-dependent manner, cell proliferation in both, RK33 and RK45 cell lines (**Figure 1A** and **1B**). Log-probit analysis of dose-response effects for CDDP and VPA allowed us to calculate the IC_{50} values for the drugs that correspond to the drug concentrations resulting in 50% inhibition of cell growth as compared to control (untreated cells), for RK33 and RK45 cell lines. The experimentally determined IC_{50} values for CDDP and VPA amounted to 1.193 ± 0.273 μg/ml, 383.4 ± 53.73 μg/ml in the RK33 and 1.387 ± 0.270 μg/ml, 449.1 ± 80.79 μg/ml in the RK45 cell lines, respectively (**Table 1**). Subsequently, log-probit analysis revealed that the dose-response effects of CDDP and VPA were not parallel to each other in both, RK33

A
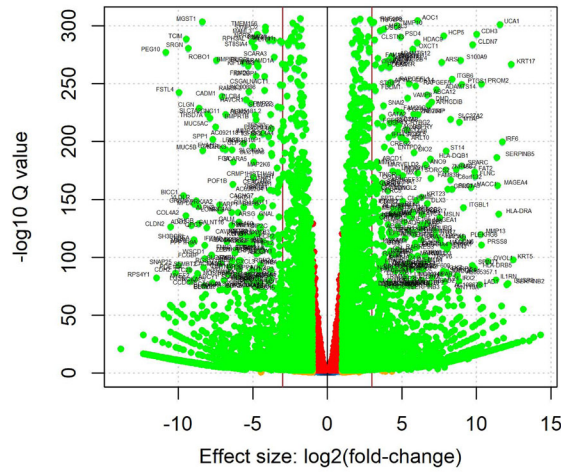
Figure 4. A. Summary of the RNASeq results. A. Volcano plot of differentially expressed genes between RK45 and RK 33 cell lines. Only the genes above the cut off values of 4 fold differential expression and *p* value of 10e-80 are annotated; B. The heatmap of top 100 differentially expressed genes. Subsequent analysis focused on assigning the top 50 up and down regulated genes to pathways and cellular processes using Enrichr (https://maayanlab.cloud/Enrichr/).

B
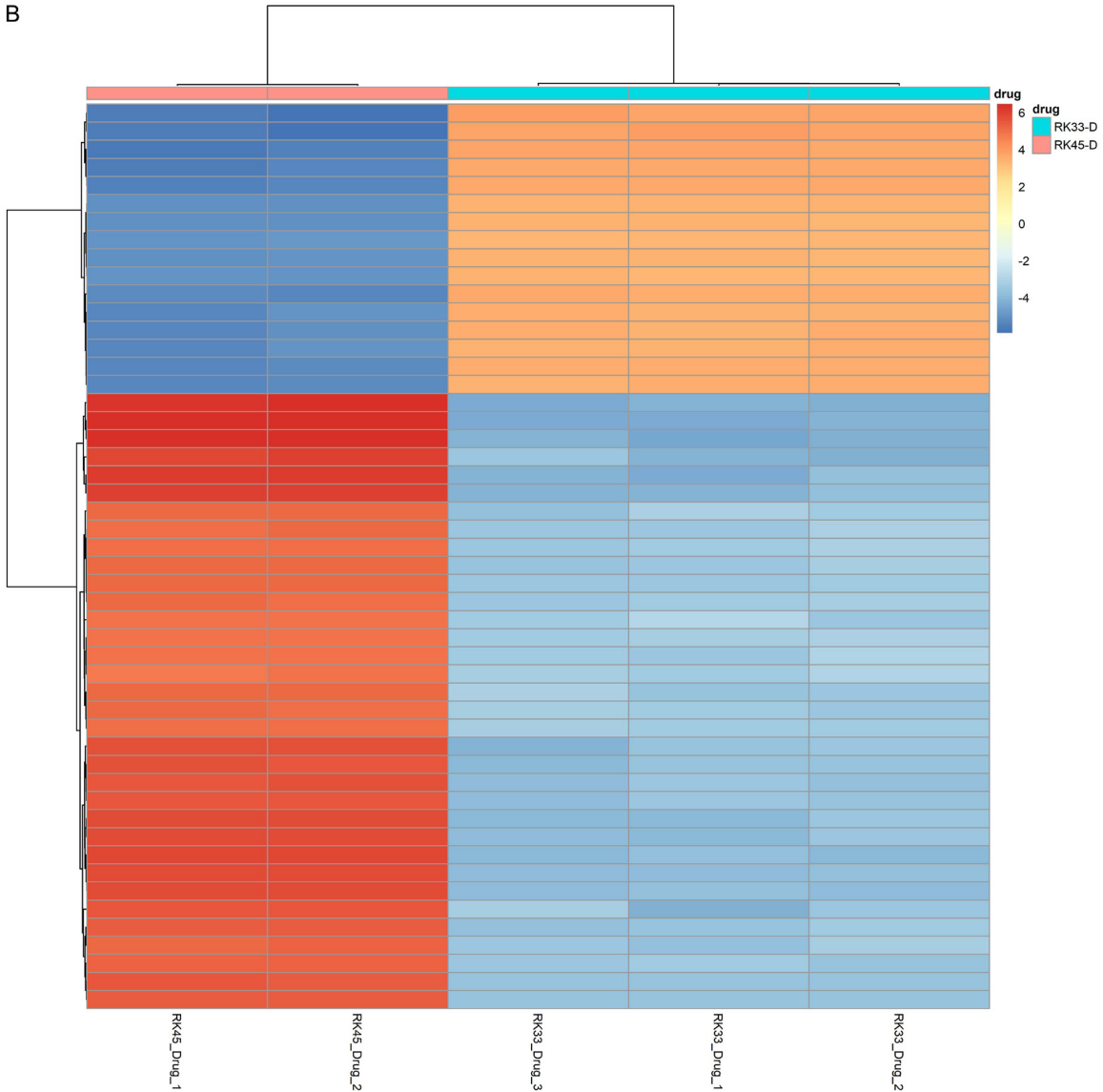
Table 3. List of up or downregulated genes of RK45 cell line after combined treatment

Downregulated genes		Upregulated genes	
	log$_2$FoldChange		log$_2$FoldChange
SGCE	-13,84760557	MYL9	14,30326644
PNMA2	-12,35660171	DSG3	13,85107829
GABRA5	-12,33556047	KRT16P6	13,5438205
CNKSR2	-12,21173859	KLK5	13,15255249
KDM5D	-12,13805586	RAB25	13,12048856
CYB5A	-12,0635145	MAGEA3	12,80732497
HHIP	-12,02808613	MT1E	12,69547702
SELENBP1	-12,01514417	CST6	12,66636448
ANO5	-11,91338551	KRT5	12,47842116
RPS6KA6	-11,86003463	DUOX1	12,41256762
RANBP17	-11,76082935	ACP5	12,38801708
RPS4XP22	-11,60433141	AEBP1	12,37841035
TSPYL5	-11,60222663	FAM83F	12,36209922
NID2	-11,56825189	KRT17	12,34971745
MEIOC	-11,46284293	THNSL2	12,34008829
RPS4Y1	-11,44578003	LINC01293	12,32318853
ARSE	-11,39754563	AL035661.1	12,26263965
ENPP4	-11,37499554	MAGEB2	12,18034298
TXLNGY	-11,32451742	DUSP2	12,12222727
DPYSL4	-11,22523154	SERPINB2	12,05732048
EFCAB10	-11,13710754	SLC7A4	12,02366764
LPAR1	-11,04344374	GTSF1	12,02109387
C4BPA	-11,01999871	KRT14	12,01170356
NOVA1	-10,99032231	TACSTD2	11,9554932
LYNX1	-10,98891478	TMEM125	11,90917869
TMEM47	-10,98801027	CD74	11,858799
ALDH7A1	-10,97237816	RNASE7	11,84423003
TTTY15	-10,95817495	CLCA2	11,83371664
AADAT	-10,95480051	BNC1	11,79928869
PEG10	-10,840852	PDLIM4	11,79139993
GUCY1A2	-10,81730421	APOBEC3G	11,77247558
CNNM1	-10,79115752	IRF6	11,75326016
EIF1AY	-10,783443	KDF1	11,72334948
NLGN4Y	-10,7559645	MDFI	11,70701504
SUSD5	-10,74012251	MXRA5	11,69777659
ITGA4	-10,71421458	PICSAR	11,67006443
BMP5	-10,69212949	SECTM1	11,64247111
CCDC198	-10,69013073	SCAT1	11,63250419
NR0B1	-10,65821143	UCA1	11,57613824
SLC40A1	-10,64411914	HLA-DRA	11,49888288
TESC	-10,64097659	APCDD1L	11,42559751
PDE3B	-10,6301273	ZBED6CL	11,42453229
CDH6	-10,56532035	MAGEA4	11,41584267
FGL1	-10,54622819	MIR205HG	11,41001817
RSPO3	-10,54060937	XAF1	11,39579505
CLDN2	-10,52023815	ARHGEF34P	11,38103987

and RK45 cell lines (**Table 1**; **Figure 1A** and **1B**).

Doses of CDDP, VPA and their mixtures (at the fixed-ratio of 1:1) were transformed into logarithms and the respective anti-proliferative effects evoked by the drugs were transformed into probits [25]. Linear regression equations for the drugs administered separately and combined in the fixed-ratio of 1:1 are presented on the graph; where y - is the probit of response, and x - is the logarithm (to the base 10) of a drug dose, R^2 - is the coefficient of determination. Test for parallelism revealed that the experimentally determined dose-response effects for CDDP and VPA are not parallel to one another in both, RK33 and RK45 cancer cell lines.

Type I isobolographic analysis revealed that the combination of CDDP with VPA (at the fixed-ratio of 1:1) produced sub-additive (antagonistic) interaction in the RK33 cell line (**Table 2**; **Figure 2A**). In this case, the experimentally-determined IC$_{50}$ $_{mix}$ value for the two-drug mixture was 383.4 ± 53.73 μg/ml and significantly differed from the additively calculated IC$_{50}$ $_{add}$ values (P<0.05; **Table 2**; **Figure 2A**). In contrast, in the RK45 cell line the same two-drug combination of CDDP with VPA (at the fixed-ratio of 1:1) exerted supra-additive (synergistic) interaction (**Table 2**; **Figure 2B**). With the Student's *t*-test, it was found that the IC$_{50 mix}$ value for the mixture of CDDP and VPA significantly differed from the additively calculated IC$_{50}$ $_{add}$ values (P<0.05; **Table 2**; **Figure 2B**).

Transcriptome analysis reveals differences in gene expression for RK33 and RK45 cells treated with VPA/CDDP combination

To explore the difference between the RK33 and RK45 response to VPA/CDDP at the molecular level, we carried out RNASeq analysis. Following the sequencing and making the count table, we used DSEQ2 algorithm to explore the differential gene expression on these samples [33]. Next, the data were visualized using Volcano plot which shows a relationship between the statistical significance and

PHF21B	-10,51489853	IVL	11,37366063
SLC1A1	-10,50118197	SERPINB5	11,37228737
GABRB3	-10,48970786	HACD4	11,35378815
KCNJ6	-10,48433184	IL1RN	11,32395366

magnitude of change in gene expression. At the false discovery rate (FDR) set to 0.005, and 4-fold minimum difference in expression, there were 2302 genes upregulated and 1793 down-regulated between the two cell lines (**Figure 4**).

GO Biological Processes database revealed that the top 50 induced genes (**Table 3**) sorted by *p*-value associated with the epidermis development. Jenses tissue annotation focused on text data mining and identifying gene names with human tissues pointed to stratified epithelium.

GWAS catalogues investigating gene to disease link on the basis of short nucleotide polymorphism (SNP) also suggest a very strong cancer connection. Finally, Human Gene Atlas analysis also pointed to epithelial as well as cancer events (**Figure 5**).

The analysis of the genes downregulated in RK45 cell line (**Table 3**), as compared to RK33, did not reveal any tractable patterns permitting one to associate these genes with a particular biological process with the exception of integrin mediated cell adhesion pathway.

Next, we investigated a possibility that the EMT process is involved in the transcriptional response to the treatment. We chose a set of characterized genes defined as EMT and involved in metastatic transition [35]. We used the list of genes provided by the authors as associated with either epithelial or mesenchymal cancer phenotype and investigated their expression in our dataset (**Table 4**). The analysis has revealed that the RK45 cell line expressed several of the genes from both lineages in high levels while the RK33 cell line does not show such changes. These data suggest that upon VPA/CCDP exposure, the RK45, but not RK33, responds by activating selected genes associated with EMT and cancer metastasis (**Figure 6**).

Combined VPA/CDDP treatment reduces the growth of RK33 and RK45 cells xenografts in Danio rerio In vivo model

To confirm the anti-cancer effects of the VPA/CDDP combined therapy against RK33 and RK45 cells, series of *in vivo* experiment on zebrafish larvae was performed. Analysis of photos obtained 24, 48, 72 and 96 h post-injection (hpi) revealed that, compared to the untreated zebrafish larvae, VPA/CDDP combined treatment significantly reduced the growth of RK33 and RK45 xenografts (**Figure 7**). The maximal reduction of cell number was observed 96 hpi for RK45 cells, where the mean xenograft size decreased approximately 11-fold in the VPA/CDDP treated group (mean = 2270 μm^2) compared to control (mean 25739 μm^2) (**Figure 7E**).

The decrease in the number of RK33 and RK45 cells in zebrafish larvae was also confirmed by qPCR analysis. After 96 h, at the tested VPA/CDDP concentration, the human *GAPDH* expression level decreased approximately 10 and 37 fold in zebrafish larvae carrying RK33 and RK45 xenografts, respectively (**Figure 7C, 7F**). Observed differences corresponded to the in vitro experiments, showing more reduced xenograft volume and human *GAPDH* expression in RK45 cells, where synergism of VPA/CDDP combined treatment was detected compared to RK33 cells (antagonism of VPA/CDDP combined treatment).

Discussion

There is a strong need for a preclinical model to identify patients that will respond to the intended treatment regimen and to test novel drugs [36]. In order to search for more effective and less toxic targeted therapies, in our study we applied a novel drug combination - CDDP, included in majority of treatment schemes of head and neck cancers, and VPA - one of the histone deacetylase inhibitors, which were proved to inhibit proliferation of different types of cancer cells, both *in vitro* and *in vivo* [17]. We have demonstrated previously that HDIs - vironostat (SAHA) and VPA are also effective against larynx cancer cells, whereas display relatively low toxicity against normal cells - primary cultures of human skin fibroblasts [13, 14].

In the present study we have determined the responses of stable cell lines derived from two patients with histologically similar larynx squamous cell carcinoma to the CDDP/VPA combined drug administration *in vitro* and *in vivo*.
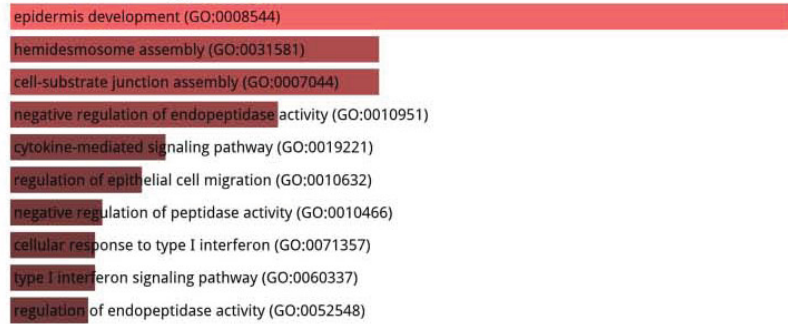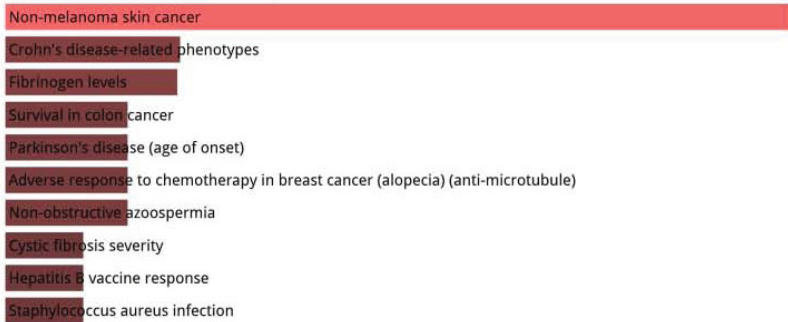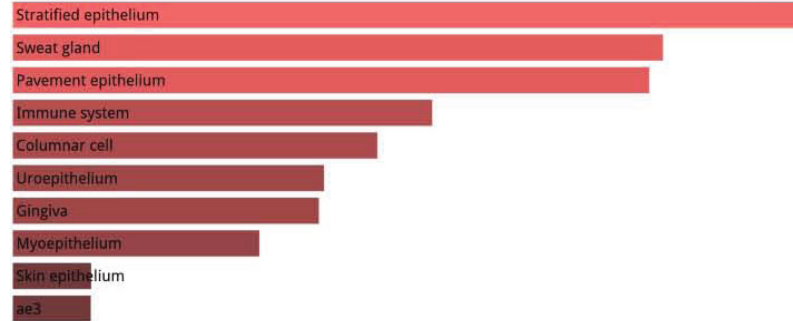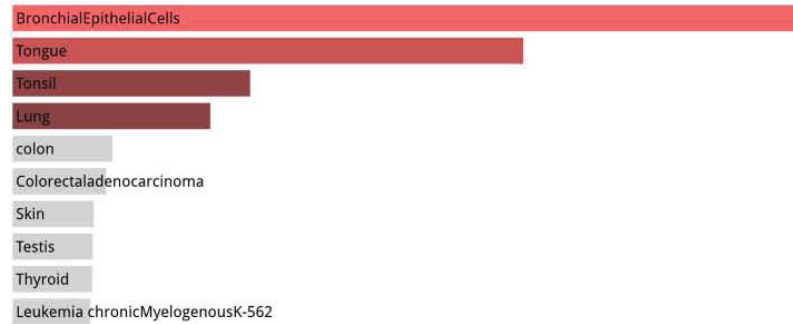
Figure 5. Graphical representation of the analysis on ENRICH server. The names of the selected database is listed about the bar graph. *P*-values below 0.05 are in gray bars.

Table 4. Upregulated genes of RK45 cell lines characteristic for epithelial and mesenchymal cancer phenotype

Epthelial genes	Mesenchymal genes
AFTPH	ACOT9
AIM1L	ANXA5
ANKRD5	AP1M1
ANXA9	AP1S2
AP1M2	ASAP1
ARHGEF16	C14orf149
ARHGEF5	C17orf51
ATP2C2	C6orf225
ATXN7L3B	C9orf21
BLCAP	CCDC88A
BSPRY	CCDC99
C17orf28	CFL2
C1orf172	CHST10
C1orf210	CTGF
C2orf15	DBN1
C6orf132	DENND5A
CAMSAP3	EIF5A2
CBLC	EMP3
CCDC64B	ETS1
CDH1	FAM101B
CDH3	FAM127A
CDS1	FERMT2
CLDN7	FEZ2
CMTM4	FGFR1
CNKSR1	FMNL3
CRB3	GLIPR1
CTSH	GNAI2
CYB561	GNG11
DDR1	GSTO1
DENND2D	HABP4
DSP	IKBIP
DTX4	KATNAL1
EFNA1	KIAA1949
ELF1	LATS2
ELF3	LEPRE1
ELMO3	LGALS1
ELOVL7	LOC100505634
EPCAM	MAP7D3
EPN3	MRC2
ESRP1	MSN
ESRP2	MSRB3
EXPH5	NMT2
F11R	OSTM1
FA2H	P4HA3
FAAH	PDLIM4
FAAH2	PGBD1
FAM108C1	PPM1F

FAM83H	PTRF
FUCA1	RAB11FIP5
FUK	RAB32
FXYD3	RRAS
GALNT3	RWDD1
GGCT	SACS
GRHL1	SCARF2
GRHL2	SGCB
HOOK1	SH2B3
HOOK2	ST3GAL2
ICA1	STX2
IDH1	SYDE1
IGSF9	TGFB1I1
ILDR1	TMEM158
INADL	TTC7B
IRF6	TTL
ITPKC	TTL
JUP	TWF2
LENG9	UROD
LIMK2	VIM
LLGL2	WTIP
LNX1	WWC2
LNX2	ZEB1
LOC440335	
LPAR2	
LSR	
MAL2	
MAP7	
MAPK13	
MARVELD2	
MARVELD3	
MKL2	
MYH14	
MYLIP	
MYO1D	
MYO5B	
MYO5C	
OVOL1	
OVOL2	
PKP3	
PLEKHG6	
PPL	
PROM2	
PRR15L	
PRRG2	
PRRG4	
PRSS8	
PTPN6	
PVRL4	
RAB11FIP4	
RASEF	

RBM47
REL
ROD1
RREB1
S100A14
SDR42E1
SH2D3A
SH3YL1
SLC15A2
SLC22A23
SLC29A2
SLC39A9
SLC44A1
SPINT1
SPINT2
SPPL3
SSH3
ST14
SYNGR2
TLCD1
TM9SF2
TMC4
TMEM125
TMEM184A
TMEM30B
TMEM79
TNK1
TSPAN13
TSTD1
WIBG
XBP1
ZFP62
ZNF552

The importance of combined use of HDIs and CDDP was demonstrated by recently published results of the phase one trial of Vorinostat (SAHA). It was used in combination with chemo-radiation therapy in the treatment of advanced staged head and neck squamous cell carcinoma, showing a complete response to this therapy in twenty four of 26 (96.2%) patients with toxicity rates comparable, if not favorable to existing therapies. This promising result resulted in recommendation for Phase II and III trials [37].

Our study has shown that cells derived from tumors with similar clinical and histological characteristic could respond differently to the same pharmacological treatment. Although the RK33 cell line was more sensitive to VPA or CDDP when they were administrated alone, the combination of both drugs did not result in synergistic anti-cancer effect. Intriguingly, combined therapy was more effective in RK45 cells, which were more resistant to the single VPA and CDDP treatments. Additionally, the suppression of cell proliferation was effective at lower individual drug concentration when administered together. Isobolographic analysis of drug-drug pharmacological interaction revealed synergism of VPA/CDDP treatment in RK45 cells, while in RK33 cells - antagonism. This tendency was also demonstrated by *in vivo* studies. Given the fact that both cell lines originate from clinically similar cases (both T3N0M0, both squamous cell carcinoma), the obtained results were surprising, while the mechanism leading to the observed differences was not understood.

To address this issue we carried out transcriptome analysis, as a part of the characterization of the molecular response of these two cell lines. The analysis of the transcriptional response has shown that RK45 but not RK33, activates genes associated with epithelial phenotype and partially involved in epithelial-to-mesenchymal transition EMT. Genes upregulated in RK45 cells and in parallel down-regulated in RK33 cells after VPA/CDDP treatment encodes proteins engaged in keratinization processes. These genes include IRF6 - a determinant of the keratinocyte proliferation-differentiation switch maintaining appropriate epidermal development [38], ST14 - involved in the terminal differentiation of keratinocytes [39] or PPL - a component of desmosomes and epidermal cornified envelope in keratinocytes, serving as a link between the cornified envelope and intracellular structural proteins [40]. Some of these proteins are Claudins - integral membrane proteins and components of tight junction strands [41], including Claudin 7 encoded by CLDN7 gene which was also upregulated after VPA/CDDP treatment. Differential expression of this gene has been reported in head and neck cancers before [42, 43]. Another examples of up-regulated genes are S100A14, encoding a protein that has been found down-regulated in cancerous tissue suggesting a tumor suppressor function [44, 45], or BLCAP,
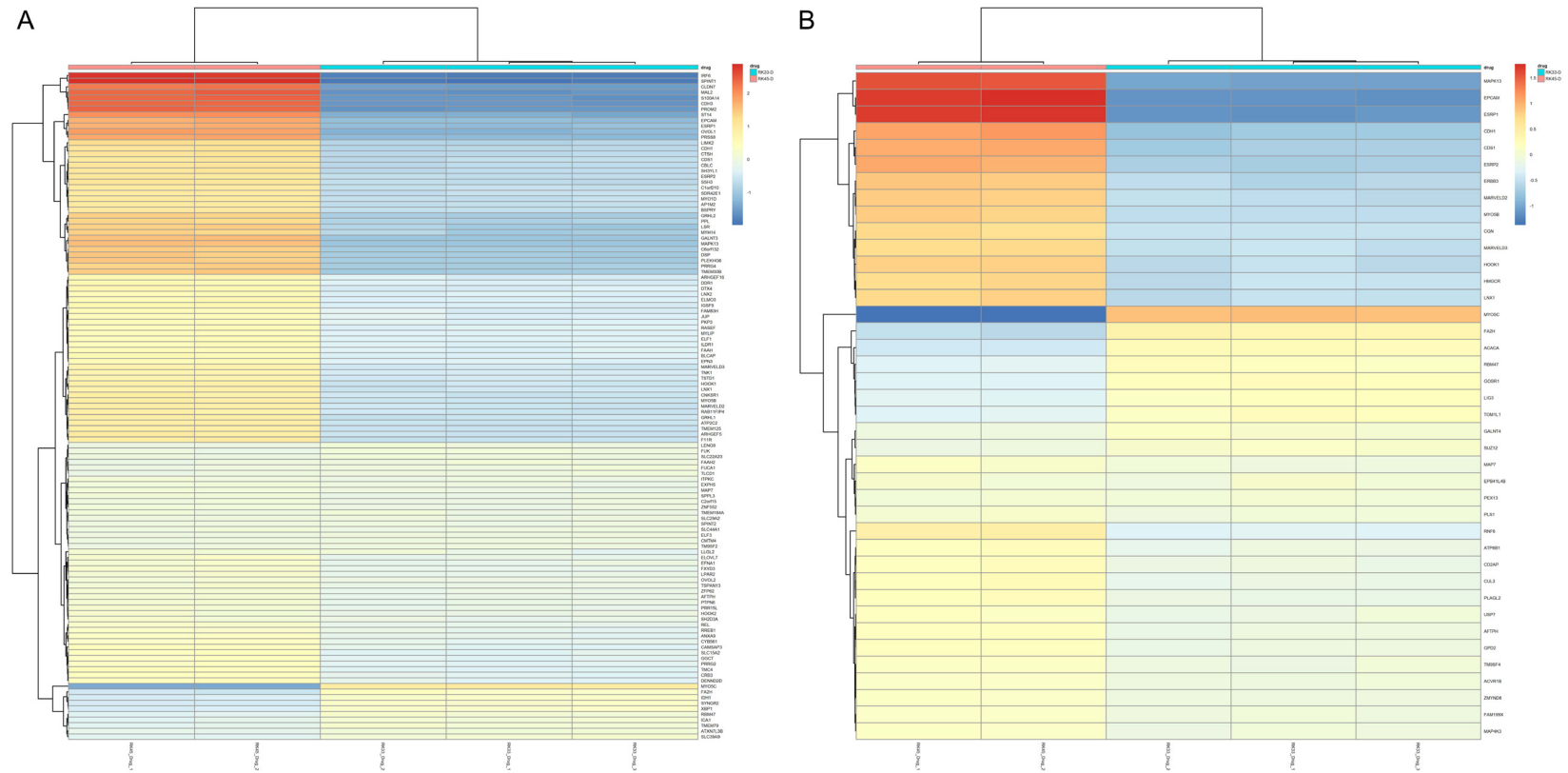
Figure 6. Heat maps of the epithelial (left panel) and mesenchymal (right panel) gene expression. The intensity gradient is from red (upregulation) to blue (down-regulation). The RK45 biological replicates are indicated with e pink bar while RK33 with the light blue bar at the top of each of the heatmaps.
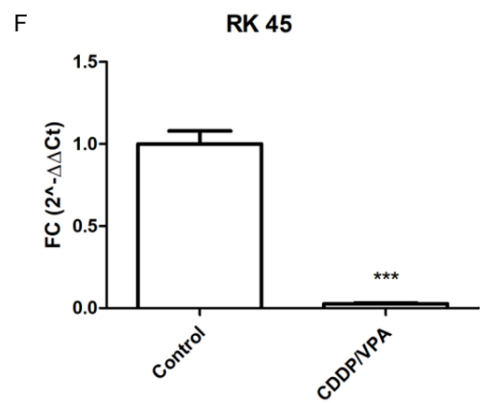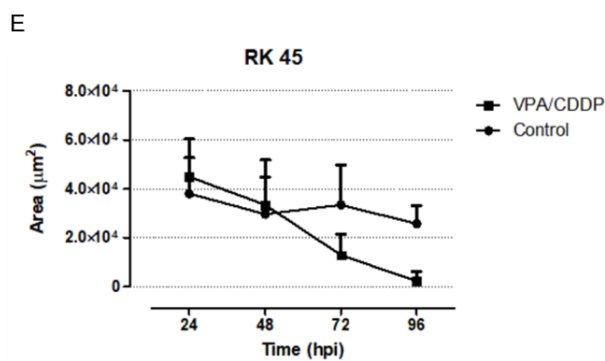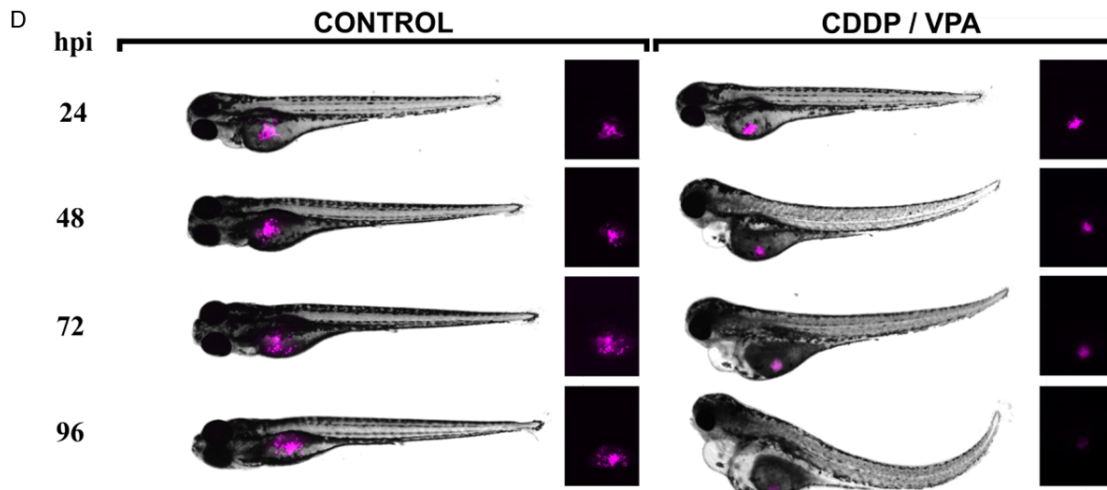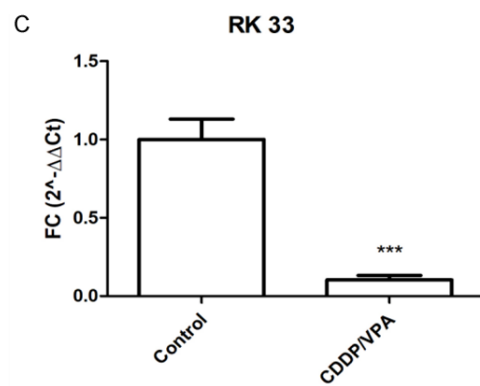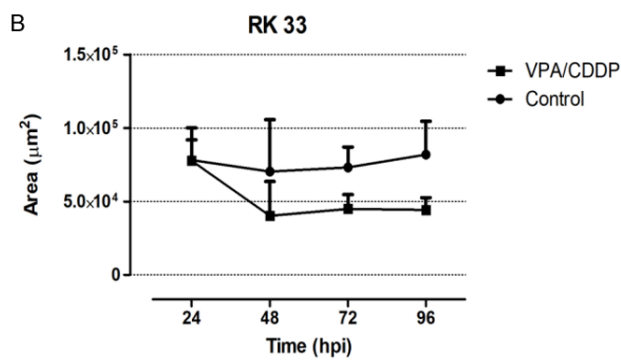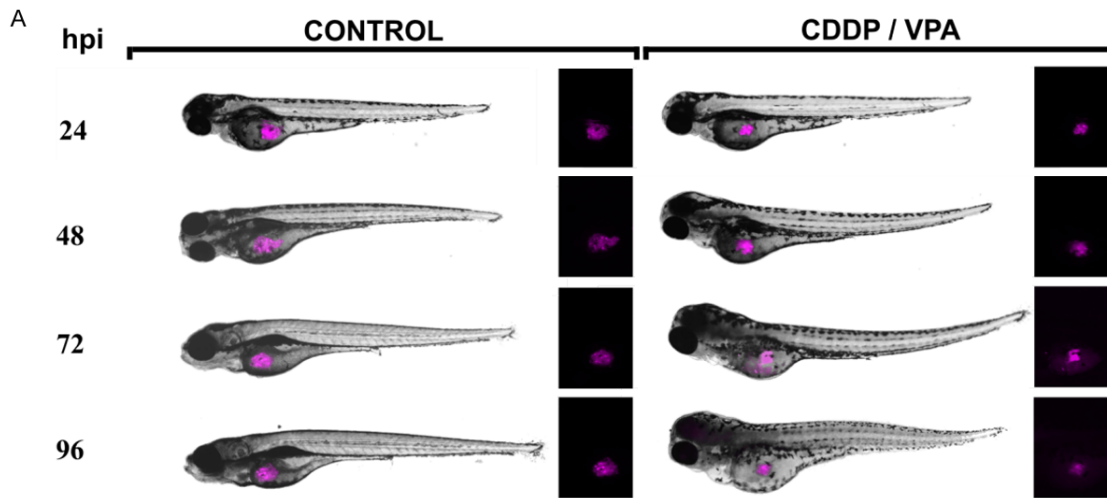
Figure 7. Effect of combined VPA/CDDP treatment on RK33 and RK45 cells xenografts in *Danio rerio* model. After injection of the xenograft, *Danio rerio* larvae were incubated at a VPA/CDDP concentration of 1/2 IC$_{50}$ (191,7 µg/ml VPA and 0.6 µg/ml CDDP for RK33 and 224,5 µg/ml VPA and 0,7 µg/ml for RK45, respectively) for 96 hours. Representative *Danio rerio* pictures taken 24, 48, 72 and 96 hours postinjection (hpi) RK33 (A) and RK45 (D) xenografts injection was shown. Untreated larvae were used as controls. Quantification of total RK33 (B) and RK44 (E) cells xenografts area (n = 5) 24, 48, 72 and 96 hpi, based on total Vybrant DiD fluorescence. The mRNA expression of human GAPDH from RK33 (C) and RK45 (F) xenofrafts determined by using qPCR method (2$^{-\Delta\Delta Ct}$) in *Danio rerio* larvae 96 hpi in the presence of VPA/CDDP compared to untreated control. The results show fold change (FC) values (mean ± SD) normalized to the fish *gapdh* gene expression. The results were analysed with one-way ANOVA test and Tukey's Multiple Comparison post hoc test (***P<0.05) were considered statistically significant.

which reduces cell growth by stimulating apoptosis via a novel mechanism independent of TP53 [46]. Finally, two of the upregulated genes in RK45 cells were CDH1 encoding E-cadherin and its placental form (CDH3), a calcium-dependent protein involved in mechanisms regulating cell-cell adhesions, mobility and proliferation of epithelial cells. Loss of function of this gene is thought to contribute to cancer progression by increasing proliferation, invasion, and/or metastasis [47]. In contrast, after VPA/CDDP treatment RK33 cells overexpressed several mesenchymal phenotype-related genes, including vimentin (VIM) that were down-regulated in RK45 cells. Both proteins, E-cadherin and VIM serves as epithelial or mesenchymal phenotype markers, respectively, and are involved in EMT processing. In our study we also found other EMT-related genes upregulated in RK33 cells, and down-regulated in RK45 cells, including ZEB1 transcription factor and FGFR1, a member of the Fibroblast Growth Factor family. Both genes are well-known inducers of EMT progression [48, 49] which could influence weak response of RK33 cells to the VPA/CDDP drug administration.

These results suggest that, while histologically similar, molecularly both cell types are very different explaining differential response for the same treatment. Based on single cell RNA sequencing, it was recently suggested that HNSCC tumors may be refined into three subtypes of cancer cells - malignant-basal, classical, and atypical, with the malignant-basal phenotype being particularly prevalent, more invasive and strongly predictive of nodal metastases [50]. Thereby, cell lines analyzed in our studies could fall into different molecular subtypes. It is tempting to speculate that RK45 might belong to atypical category and RK 33 to classical but further work will be necessary to confirm this hypothesis. Additionally, multiclonal composition of the cancer cell lines, of which the line RK45 comprised neoplastic cellular clones more sensitive to the combination

of CDDP with VPA, could at some extent contribute to the observed phenomena of drug interaction - synergism versus antagonism.

Although all the above-mentioned suggestions could readily explain the observed differences in the anti-proliferative effects for the combination of CDDP with VPA, more biomolecular studies are needed to reveal this phenomenon.

Acknowledgements

Disclosure of conflict of interest

None.

Address correspondence to: Andrzej Stepulak, Department of Biochemistry and Molecular Biology, Medical University of Lublin, Chodźki 1, 20-093 Lublin, Poland. Tel: (+48) 81 448 6358; Fax: (+48) 81 448 6352; E-mail: andrzej.stepulak@umlub.pl

References

[1] Steuer CE, El-Deiry M, Parks JR, Higgins KA and Saba NF. An update on larynx cancer. CA Cancer J Clin 2017; 67: 31-50.

[2] Department of Veterans Affairs Laryngeal Cancer Study Group, Wolf GT, Fisher SG, Hong WK, Hillman R, Spaulding M, Laramore GE, Endicott JW, McClatchey K and Henderson WG. Induction chemotherapy plus radiation compared with surgery plus radiation in patients with advanced laryngeal cancer. N Engl J Med 1991; 324: 1685-1690.

[3] Vokes EE. Competing roads to larynx preservation. J Clin Oncol 2013; 31: 833-835.

[4] Blanchard P, Baujat B, Holostenco V, Bourredjem A, Baey C, Bourhis J and Pignon JP; MACH-CH Collaborative group. Meta-analysis of chemotherapy in head and neck cancer (MACH-NC): a comprehensive analysis by tumour site. Radiother Oncol 2011; 100: 33-40.

[5] Fung C, Dinh P Jr, Ardeshir-Rouhani-Fard S, Schaffer K, Fossa SD and Travis LB. Toxicities associated with cisplatin-based chemotherapy and radiotherapy in long-term testicular cancer survivors. Adv Urol 2018; 2018: 8671832.

[6] Ferris RL, Saba NF, Gitlitz BJ, Haddad R, Sukari A, Neupane P, Morris JC, Misiukiewicz K, Bauman JE, Fenton M, Jimeno A, Adkins DR, Schneider CJ, Sacco AG, Shirai K, Bowles DW, Gibson M, Nwizu T, Gottardo R, Manjarrez KL, Dietsch GN, Bryan JK, Hershberg RM and Cohen EEW. Effect of adding motolimod to standard combination chemotherapy and cetuximab treatment of patients with squamous cell carcinoma of the head and neck: the active8 randomized clinical trial. JAMA Oncol 2018; 4: 1583-1588.

[7] Bonner JA, Harari PM, Giralt J, Cohen RB, Jones CU, Sur RK, Raben D, Baselga J, Spencer SA, Zhu J, Youssoufian H, Rowinsky EK and Ang KK. Radiotherapy plus cetuximab for locoregionally advanced head and neck cancer: 5-year survival data from a phase 3 randomised trial, and relation between cetuximab-induced rash and survival. Lancet Oncol 2010; 11: 21-28.

[8] Ang KK, Zhang Q, Rosenthal DI, Nguyen-Tan PF, Sherman EJ, Weber RS, Galvin JM, Bonner JA, Harris J, El-Naggar AK, Gillison ML, Jordan RC, Konski AA, Thorstad WL, Trotti A, Beitler JJ, Garden AS, Spanos WJ, Yom SS and Axelrod RS. Randomized phase III trial of concurrent accelerated radiation plus cisplatin with or without cetuximab for stage III to IV head and neck carcinoma: RTOG 0522. J Clin Oncol 2014; 32: 2940-2950.

[9] Winquist E, Agbassi C, Meyers BM, Yoo J and Chan KKW; Head and Neck Disease Site Group. Systemic therapy in the curative treatment of head and neck squamous cell cancer: a systematic review. J Otolaryngol Head Neck Surg 2017; 46: 29.

[10] Audia JE and Campbell RM. Histone modifications and cancer. Cold Spring Harb Perspect Biol 2016; 8: a019521.

[11] Castilho RM, Squarize CH and Almeida LO. Epigenetic modifications and head and neck cancer: implications for tumor progression and resistance to therapy. Int J Mol Sci 2017; 18: 1506.

[12] Li Y and Seto E. HDACs and HDAC inhibitors in cancer development and therapy. Cold Spring Harb Perspect Med 2016; 6: a026831.

[13] Grabarska A, Jeleniewicz M and Kiełbus JM, Nowosadzka E, Rivero-Muller A, Polberg K and Stepulak A. Valproic acid suppresses growth and enhances cisplatin cytotoxicity to larynx cancer cells. Head Neck Oncol 2014; 3: 7.

[14] Grabarska A, Luszczki JJ, Nowosadzka E, Gumbarewicz E, Jeleniewicz W, Dmoszynska-

Graniczka M, Kowalczuk K, Kupisz K, Polberg K and Stepulak A. Histone deacetylase inhibitor SAHA as potential targeted therapy agent for larynx cancer cells. J Cancer 2017; 8: 19-28.

[15] Erlich RB, Rickwood D, Coman WB, Saunders NA and Guminski A. Valproic acid as a therapeutic agent for head and neck squamous cell carcinomas. Cancer Chemother Pharmacol 2009; 63: 381-389.

[16] Lipska K, Gumieniczek A and Filip AA. Anticonvulsant valproic acid and other short-chain fatty acids as novel anticancer therapeutics: possibilities and challenges. Acta Pharm 2020; 70: 291-301.

[17] Wawruszak A, Kalafut J, Okon E, Czapinski J, Halasa M, Przybyszewska A, Miziak P, Okla K, Rivero-Muller A and Stepulak A. Histone deacetylase inhibitors and phenotypical transformation of cancer cells. Cancers (Basel) 2019; 11: 148.

[18] Chen JH, Zheng YL, Xu CQ, Gu LZ, Ding ZL, Qin L, Wang Y, Fu R, Wan YF and Hu CP. Valproic acid (VPA) enhances cisplatin sensitivity of non-small cell lung cancer cells via HDAC2 mediated down regulation of ABCA1. Biol Chem 2017; 398: 785-792.

[19] Lee H, Lee JY, Ha DH, Jeong JH and Park JB. Effects of valproic acid on morphology, proliferation, and differentiation of mesenchymal stem cells derived from human gingival tissue. Implant Dent 2018; 27: 33-42.

[20] Jiang W, Zheng Y, Huang Z, Wang M, Zhang Y, Wang Z, Jin X and Xia Q. Role of SMAD4 in the mechanism of valproic acid's inhibitory effect on prostate cancer cell invasiveness. Int Urol Nephrol 2014; 46: 941-946.

[21] Brunn J, Wiroth V, Kowalski M, Runge U and Sabolek M. Valproic acid in normal therapeutic concentration has no neuroprotective or differentiation influencing effects on long term expanded murine neural stem cells. Epilepsy Res 2014; 108: 623-633.

[22] Georgoff PE, Nikolian VC, Bonham T, Pai MP, Tafatia C, Halaweish I, To K, Watcharotone K, Parameswaran A, Luo R, Sun D and Alam HB. Safety and tolerability of intravenous valproic acid in healthy subjects: a phase I dose-escalation trial. Clin Pharmacokinet 2018; 57: 209-219.

[23] Caponigro F, Di Gennaro E, Ionna F, Longo F, Aversa C, Pavone E, Maglione MG, Di Marzo M, Muto P, Cavalcanti E, Petrillo A, Sandomenico F, Maiolino P, D'Aniello R, Botti G, De Cecio R, Losito NS, Scala S, Trotta A, Zotti AI, Bruzzese F, Daponte A, Calogero E, Montano M, Pontone M, De Feo G, Perri F and Budillon A. Phase II clinical study of valproic acid plus cisplatin and cetuximab in recurrent and/or metastatic squamous cell carcinoma of Head and Neck-V-CHANCE trial. BMC Cancer 2016; 16: 918.

[24] Rzeski W, Paduch R, Klatka J, Kandefer-Szerszen M, Stepulak A, Pozarowski P and Zdzisinska B. Establishment and preliminary characterization of two cell lines derived from larynx carcinoma. Folia Histochem Cytobiol 2002; 40: 195-196.

[25] Litchfield JT Jr and Wilcoxon F. A simplified method of evaluating dose-effect experiments. J Pharmacol Exp Ther 1949; 96: 99-113.

[26] Luszczki JJ. Isobolographic analysis of interaction between drugs with nonparallel dose-response relationship curves: a practical application. Naunyn Schmiedebergs Arch Pharmacol 2007; 375: 105-114.

[27] Tallarida RJ. Revisiting the isobole and related quantitative methods for assessing drug synergism. J Pharmacol Exp Ther 2012; 342: 2-8.

[28] Greco WR, Bravo G and Parsons JC. The search for synergy: a critical review from a response surface perspective. Pharmacol Rev 1995; 47: 331-385.

[29] Wawruszak A, Luszczki JJ, Grabarska A, Gumbarewicz E, Dmoszynska-Graniczka M, Polberg K and Stepulak A. Assessment of interactions between cisplatin and two histone deacetylase inhibitors in MCF7, T47D and MDA-MB-231 human breast cancer cell lines - an isobolographic analysis. PLoS One 2015; 10: e0143013.

[30] Tallarida RJ, Porreca F and Cowan A. Statistical-analysis of drug-drug and site-site interactions with isobolograms. Life Sciences 1989; 45: 947-961.

[31] Kim D, Paggi JM, Park C, Bennett C and Salzberg SL. Graph-based genome alignment and genotyping with HISAT2 and HISAT-genotype. Nat Biotechnol 2019; 37: 907-915.

[32] Anders S, Pyl PT and Huber W. HTSeq--a Python framework to work with high-throughput sequencing data. Bioinformatics 2015; 31: 166-169.

[33] Love MI, Huber W and Anders S. Moderated estimation of fold change and dispersion for RNA-seq data with DESeq2. Genome Biol 2014; 15: 550.

[34] Naakka E, Tuomainen K, Wistrand H, Palkama M, Suleymanova I, Al-Samadi A and Salo T. Fully human tumor-based matrix in three-dimensional spheroid invasion assay. J Vis Exp 2019.

[35] Zhao M, Kong L, Liu Y and Qu H. dbEMT: an epithelial-mesenchymal transition associated gene resource. Sci Rep 2015; 5: 11459.

[36] Dohmen AJ, Swartz JE, Van Den Brekel MW, Willems SM, Spijker R, Neefjes J and Zuur CL. Feasibility of primary tumor culture models and preclinical prediction assays for head and neck cancer: a narrative review. Cancers (Basel) 2015; 7: 1716-1742.

[37] Teknos TN, Grecula J, Agrawal A, Old MO, Ozer E, Carrau R, Kang S, Rocco J, Blakaj D, Diavolitsis V, Kumar B, Kumar P, Pan Q, Palettas M, Wei L, Baiocchi R and Savvides P. A phase 1 trial of Vorinostat in combination with concurrent chemoradiation therapy in the treatment of advanced staged head and neck squamous cell carcinoma. Invest New Drugs 2019; 37: 702-710.

[38] Richardson RJ, Dixon J, Malhotra S, Hardman MJ, Knowles L, Boot-Handford RP, Shore P, Whitmarsh A and Dixon MJ. Irf6 is a key determinant of the keratinocyte proliferation-differentiation switch. Nat Genet 2006; 38: 1329-1334.

[39] Chen YW, Wang JK, Chou FP, Chen CY, Rorke EA, Chen LM, Chai KX, Eckert RL, Johnson MD and Lin CY. Regulation of the matriptase-prostasin cell surface proteolytic cascade by hepatocyte growth factor activator inhibitor-1 during epidermal differentiation. J Biol Chem 2010; 285: 31755-31762.

[40] Groot KR, Sevilla LM, Nishi K, DiColandrea T and Watt FM. Kazrin, a novel periplakin-interacting protein associated with desmosomes and the keratinocyte plasma membrane. J Cell Biol 2004; 166: 653-659.

[41] Diaz-Coranguez M, Liu X and Antonetti DA. Tight junctions in cell proliferation. Int J Mol Sci 2019; 20: 5972.

[42] Karpathiou G, Stachowitz ML, Dumollard JM, Gavid M, Froudarakis M, Prades JM and Peoc'h M. Gene expression comparison between the primary tumor and its lymph node metastasis in head and neck squamous cell carcinoma: a pilot study. Cancer Genomics Proteomics 2019; 16: 155-161.

[43] Zhou S, Piao X, Wang C, Wang R and Song Z. Identification of claudin1, 3, 7 and 8 as prognostic markers in human laryngeal carcinoma. Mol Med Rep 2019; 20: 393-400.

[44] Kim G, Chung JY, Jun SY, Eom DW, Bae YK, Jang KT, Kim J, Yu E and Hong SM. Loss of S100A14 expression is associated with the progression of adenocarcinomas of the small intestine. Pathobiology 2013; 80: 95-101.

[45] Sapkota D, Costea DE, Blo M, Bruland O, Lorens JB, Vasstrand EN and Ibrahim SO. S100A14 inhibits proliferation of oral carcinoma derived cells through G1-arrest. Oral Oncol 2012; 48: 219-225.

[46] Yao J, Duan L, Fan M, Yuan J and Wu X. Overexpression of BLCAP induces S phase arrest and apoptosis independent of p53 and NF-kappaB in human tongue carcinoma: BLCAP overexpression induces S phase arrest and apoptosis. Mol Cell Biochem 2007; 297: 81-92.

[47] Bruner HC and Derksen PWB. Loss of E-cadherin-dependent cell-cell adhesion and the development and progression of cancer. Cold Spring Harb Perspect Biol 2018; 10: a029330.

[48] Zhang P, Sun Y and Ma L. ZEB1: at the crossroads of epithelial-mesenchymal transition, metastasis and therapy resistance. Cell Cycle 2015; 14: 481-487.

[49] Katoh M and Nakagama H. FGF receptors: cancer biology and therapeutics. Med Res Rev 2014; 34: 280-300.

[50] Puram SV, Tirosh I, Parikh AS, Patel AP, Yizhak K, Gillespie S, Rodman C, Luo CL, Mroz EA, Emerick KS, Deschler DG, Varvares MA, Mylvaganam R, Rozenblatt-Rosen O, Rocco JW, Faquin WC, Lin DT, Regev A and Bernstein BE. Single-cell transcriptomic analysis of primary and metastatic tumor ecosystems in head and neck cancer. Cell 2017; 171: 1611-1624, e1624.